J Arid Land (2023) 15(3): 253–273
https://doi.org/10.1007/s40333-023-0052-1

Science Press Springer-Verlag

# Driving forces behind the spatiotemporal heterogeneity of land-use and land-cover change: A case study of the Weihe River Basin, China

WU Jingyan, LUO Jungang*, ZHANG Han, YU Mengjie

State Key Laboratory of Eco-hydraulics in Northwest Arid Region, Xi'an University of Technology, Xi'an 710048, China

**Abstract:** The impact of socioeconomic development on land-use and land-cover change (LUCC) in river basins varies spatially and temporally. Exploring the spatiotemporal evolutionary trends and drivers of LUCC under regional disparities is the basis for the sustainable development and management of basins. In this study, the Weihe River Basin (WRB) in China was selected as a typical basin, and the WRB was divided into the upstream of the Weihe River Basin (UWRB), the midstream of the Weihe River Basin (MWRB), the downstream of the Weihe River Basin (DWRB), the Jinghe River Basin (JRB), and the Luohe River Basin (LRB). Based on land-use data (cultivated land, forestland, grassland, built-up land, bare land, and water body) from 1985 to 2020, we analyzed the spatiotemporal heterogeneity of LUCC in the WRB using a land-use transfer matrix and a dynamic change model. The driving forces of LUCC in the WRB in different periods were detected using the GeoDetector, and the selected influencing factors included meteorological factors (precipitation and temperature), natural factors (elevation, slope, soil, and distance to rivers), social factors (distance to national highway, distance to railway, distance to provincial highway, and distance to expressway), and human activity factors (population density and gross domestic product (GDP)). The results indicated that the types and intensities of LUCC conversions showed considerable disparities across different sub-basins, where complex conversions among cultivated land, forestland, and grassland occurred in the LRB, JRB, and UWRB, with higher dynamic change before 2000. The conversion of other land-use types to built-up land was concentrated in the UWRB, MWRB, and DWRB, with substantial increases after 2000. Additionally, the driving effects of the influencing factors on LUCC in each sub-basin also exhibited distinct diversity, with the LRB and JRB being influenced by the meteorological and social factors, and the UWRB, MWRB, and DWRB being driven by human activity factors. Moreover, the interaction of these influencing factors indicated an enhanced effect on LUCC. This study confirmed the spatiotemporal heterogeneity effects of socioeconomic status on LUCC in the WRB under regional differences, contributing to the sustainable development of the whole basin by managing sub-basins according to local conditions.

**Keywords:** land-use and land-cover change (LUCC); spatial heterogeneity; land-use conversion; dynamic change model; GeoDetector; human activities; Weihe River Basin

**Citation:** WU Jingyan, LUO Jungang, ZHANG Han, YU Mengjie. 2023. Driving forces behind the spatiotemporal heterogeneity of land-use and land-cover change: A case study of the Weihe River Basin, China. Journal of Arid Land, 15(3): 253–273. https://doi.org/10.1007/s40333-023-0052-1

*Corresponding author: LUO Jungang (E-mail: jgluo@xaut.edu.cn)
Received 2022-05-27; revised 2022-12-22; accepted 2022-12-26

## 1 Introduction

Land is an important component of human survival and development (Wulder et al., 2008; Song et al., 2021). Land-use and land-cover change (LUCC) is affected by the integrative actions of nature, society, and economy at different temporal and spatial scales (Wei et al., 2021; Wu et al., 2021). Especially for river basins, LUCC can impact the hydrological cycle processes (Du and Shi, 2012; Ning et al., 2018; Nhi et al., 2022). A full understanding of the spatiotemporal heterogeneity of LUCC in river basins are essential to defend against a series of extreme hydrological events (Jiang et al., 2021; Omer et al., 2021). Therefore, exploring the spatiotemporal heterogeneity and driving mechanisms of LUCC in river basins is essential for their sustainable development.

Analysis of the spatiotemporal heterogeneity of LUCC is the basis of scientific understanding of the formation mechanisms of LUCC and its distribution characteristics (Nie et al., 2021; Wei et al., 2021; Wu et al., 2021). Methods such as the land-use transfer matrix and dynamic change model can reveal the spatiotemporal heterogeneity of land use in both time and space. For example, Ning et al. (2018) revealed the spatiotemporal heterogeneity of LUCC in China. Wei et al. (2021) used a land-use transfer matrix and a dynamic change model to reveal the spatiotemporal pattern change of land use in a glacially affected area in the Tianshan Mountains. In previous studies, it has always been challenging to discuss the regional characteristics of LUCC (Wei et al., 2021). Different land-use patterns and uneven economic development have influenced the spatial distribution of land use (Wu et al., 2021). The Hu Huanyong Line represents the demarcation line of population development level and socioeconomic structure in China (Chen et al., 2016). LUCC shows significant spatiotemporal heterogeneity in regions across this line (Kong et al., 2022). However, there are few studies on LUCC in these regions, especially at the river basin scale. Therefore, it is essential to explore the impact of regional differences on LUCC in river basins around the Hu Huanyong Line.

At the river basin scale, LUCC is a dynamic process involving spatiotemporal heterogeneity in its determinants and drivers, and the driving mechanisms become more complex as the river basin evolves (Hasselmann et al., 2010; Batunacun et al., 2018). Therefore, it is necessary to explore the main drivers of LUCC according to its spatiotemporal heterogeneity. This can explain the intrinsic causes and extrinsic factors of LUCC and provide a reference for future trends in the evolution of land-use patterns (Shaharum et al., 2018; Kindu et al., 2020). The methods used for the detection of the driving forces of LUCC include geographically weighted regression, random forest, and GeoDetector (Zhou et al., 2020; Guo et al., 2021; Wang et al., 2021). GeoDetector has the unique advantage of dealing with spatially hierarchical heterogeneous features and revealing the driving role of the influencing factors (Song et al., 2020). Previous studies have applied GeoDetector to extensively investigate the driving effects of various factors on LUCC (Wang et al., 2021; Wei et al., 2022; Wu et al., 2022a). However, systematic research on the spatiotemporal heterogeneity of the LUCC drivers in the special geographic area divided by the Hu Huanyong Line is still lacking in existing studies.

Therefore, this study attempts to reveal the spatiotemporal heterogeneity and complex driving mechanisms of LUCC in river basins around the Hu Huanyong Line. The Weihe River Basin (WRB) is crossed by the Hu Huanyong Line. Uneven economic development and regional differences in the WRB have a great impact on LUCC. Therefore, this study aims to (1) reveal the evolutionary trends in the spatiotemporal pattern of land use in the WRB using a land-use transfer matrix and a dynamic change model; (2) identify the driving forces of LUCC by selecting relevant factors from both natural environment and social economy in the WRB by GeoDetector; and (3) explore the driving mechanisms behind the formation of the spatiotemporal heterogeneity of LUCC in the WRB. This study is important for the improvement of ecological environment and the control of hydrological extremes in the WRB, and the results can provide a scientific basis for future land-use planning and management in the WRB.

## 2 Materials and methods

### 2.1 Study area

The Weihe River is the largest tributary of the Yellow River in China, with a length of 818.00 km and a basin area of 134,766.00 km$^2$ (Wu et al., 2022b). The longitude of the WRB is from 104°00′E to 110°20′E, and the latitude is from 33°50′N to 38°00′N. The topography is high in the west, north, and south, and low in the east and middle. The WRB has a temperate monsoon climate, with average annual temperature of 7.80°C–13.50°C and average annual precipitation of 400.00–800.00 mm (Du and Shi, 2012; Wu et al., 2022a). The WRB includes five sub-basins: the upstream of the Weihe River Basin (UWRB), the midstream of the Weihe River Basin (MWRB), the downstream of the Weihe River Basin (DWRB), the Jinghe River Basin (JRB), and the Luohe River Basin (LRB). The Hu Huanyong Line crosses the WRB. Influenced by geographical location and socioeconomic factors, the land-use patterns in different sub-basins have obvious spatiotemporal differences. The geographical location and division of the WRB are shown in Figure 1.

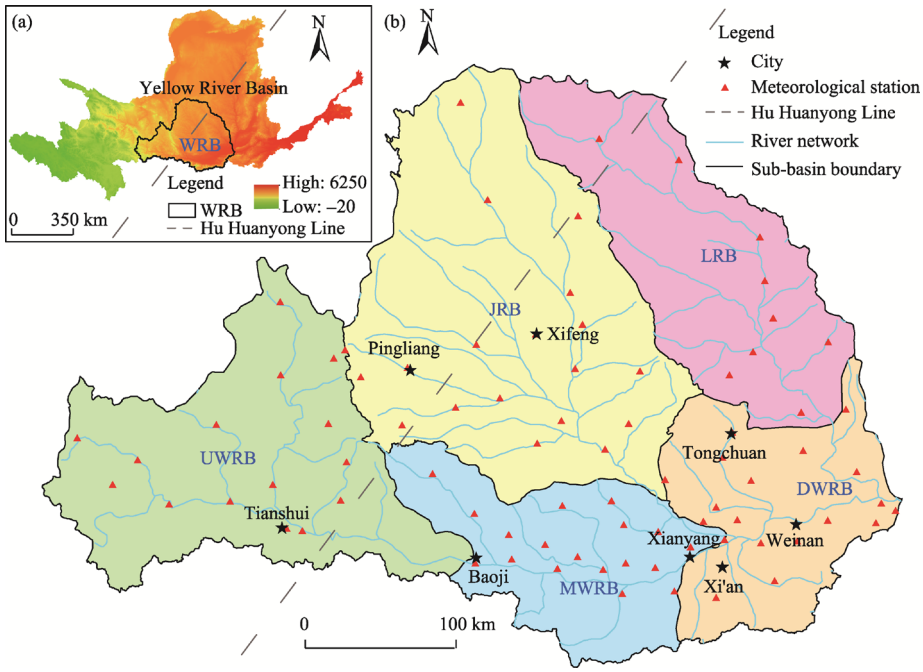


**Fig. 1** Geographical location of the Weihe River Basin (WRB) in the Yellow River Basin (a) and overview of the WRB and its sub-basins (b). UWRB, the upstream of the Weihe River Basin; MWRB, the midstream of the Weihe River Basin; DWRB, the downstream of the Weihe River Basin; JRB, Jinghe River Basin; LRB, Luohe River Basin.

### 2.2 Data sources

The principal data in this study include the datasets of LUCC, meteorological factors, natural factors, social factors, and human activity factors. The LUCC dataset was obtained from the Big Earth Data Science Engineering Program (https://data.casearth.cn), which used all Landsat TM/ETM/OLI remote sensing images from 1984 to 2020 as the chief data source to produce a 30-m fine surface coverage dynamic monitoring product from 1985 to 2020 with an interval of 5 a, based on a combination of change detection and dynamic updates (Zhang et al., 2021). According to land resource attributes and land-use patterns (Sun et al., 2018), we obtained six land-use types in the WRB: cultivated land, forestland, grassland, built-up land, bare land, and water body. The classification quality was verified by random sampling and high-resolution

historical images from Google Earth (Zhan et al., 2021), with an average Kappa coefficient of 0.83.

The datasets of meteorological factors, including annual precipitation and annual average temperature, were derived from the National Meteorological Science Data Center (https://data.cma.cn) and rasterized by spatial interpolation. The datasets of natural factors, comprising elevation, slope, soil, and distance from the river, were collected from the Geospatial Data Cloud (http://www.gscloud.cn) and Resource and Environment Science and Data Center (RESDC; https://www.resdc.cn). Social factors included distance information from traffic (national highway, provincial highway, expressway, and railway), and the datasets were provided by the National Cryosphere Desert Data Center (http://www.ncdc.ac.cn). Distance information was obtained from vector data using Euclidean distance processing. The datasets of human activity factors from the RESDC included population density and gross domestic product (GDP). Furthermore, the LUCC, elevation, and slope data were uniformly processed into 30 m raster data by resampling and spatial interpolation techniques. The panel data of LUCC and its influencing factors were obtained by extracting values to points in ArcMap spatial analysis toolbox. Details of the data are presented in Table 1.

**Table 1** Details of the datasets of land-use and land-cover change (LUCC) and its influencing factors

| Category | Parameter | Type | Scale/resolution | Period | Data source |
|---|---|---|---|---|---|
| Land use | LUCC | Raster | 30 m×30 m | 1985–2020 (interval of 5 a) | Big Earth Data Science Engineering Program (https://data.casearth.cn) |
| Meteorological factors | Precipitation | Numeric | Annual | 1980–2019 | National Meteorological Science Data Center (https://data.cma.cn) |
| | Temperature | Numeric | Annual | 1980–2019 | |
| Natural factors | Elevation (DEM) | Raster | 30 m×30 m | 2009 | Geospatial Data Cloud (http://www.gscloud.cn) |
| | Slope | Raster | 30 m×30 m | 2009 | |
| | Soil | Raster | 1000 m×1000 m | 2010 | Resource and Environment Science and Data Center (https://www.resdc.cn) |
| | Distance to rivers | Vector | 1:250,000 | 2015 | |
| Social factors | Distance to national highway | Vector | 1:250,000 | 2015 | National Cryosphere Desert Data Center (http://www.ncdc.ac.cn) |
| | Distance to railway | Vector | 1:250,000 | 2015 | |
| | Distance to provincial highway | Vector | 1:250,000 | 2015 | |
| | Distance to expressway | Vector | 1:250,000 | 2015 | |
| Human activity factors | Population density | Raster | 1000 m×1000 m | 1985–2015 (interval of 5 a) | Resource and Environment Science and Data Center (https://www.resdc.cn) |
| | Gross domestic product (GDP) | Raster | 1000 m×1000 m | 1985–2015 (interval of 5 a) | |

## 2.3 Methods

### 2.3.1 Transfer matrix method

The land-use transfer matrix can express the change direction and quantity structure characteristics of each land-use type and reflect the mutual conversion relationship between land-use types (Yang et al., 2022). The transfer matrix can effectively illustrate the change in land-use types for each period in the study area, and the formula is given by Equation 1.

$$S_{ij} = \begin{bmatrix} S_{11} & \cdots & S_{1n} \\ \vdots & \ddots & \vdots \\ S_{n1} & \cdots & S_{nn} \end{bmatrix}, \quad (1)$$

where $S_{ij}$ indicates the number of land-use type $i$ converted to land-use type $j$ in a certain period; and $n$ represents the total number of land-use types.

### 2.3.2 Dynamic change model

LUCC can be described by the dynamic change model, which includes comprehensive land-use dynamic index and single land-use dynamic index (comprising relative land-use dynamic index and absolute land-use dynamic index), each of which expresses different characteristics of LUCC (Wei et al., 2021).

The comprehensive land-use dynamic index can be used to reflect the intensity of the overall change in land-use quantity over a certain period within the study area. It was calculated using Equation 2.

$$\mathrm{CLUDI}=\frac{\sum_{i=1}^{n}\left(M_{bi}-M_{ai}\right)}{S}\times\frac{1}{T}\times 100\%, \tag{2}$$

where CLUDI denotes the comprehensive land-use dynamic index (%); $M_{ai}$ and $M_{bi}$ denote the area of land-use type $i$ in the initial stage $a$ and final stage $b$ within the study area ($km^2$), respectively; $S$ is the area of the study area ($km^2$); and $T$ is the length of the study period (a).

The relative land-use dynamic index can effectively describe the activity of a certain land-use type, which can be calculated using Equation 3.

$$\mathrm{RLUDI}_i=\frac{\Delta M_{\mathrm{in}}+\Delta M_{\mathrm{out}}}{M_{ai}}\times\frac{1}{T}\times 100\%, \tag{3}$$

where $\mathrm{RLUDI}_i$ denotes the relative land-use dynamic index (%); $\Delta M_{\mathrm{in}}$ represents the area of other land-use types converted to land-use type $i$ ($km^2$); and $\Delta M_{\mathrm{out}}$ represents the area of land-use type $i$ converted to other land-use types ($km^2$).

The absolute land-use dynamic index can directly reflect the quantitative change range of a certain land-use type within a certain period in the study area. It can be calculated using Equation 4.

$$\mathrm{ALUDI}_i=\frac{M_{bi}-M_{ai}}{M_{ai}}\times\frac{1}{T}\times 100\%, \tag{4}$$

where $\mathrm{ALUDI}_i$ denotes the absolute land-use dynamic index (%).

### 2.3.3 GeoDetector

The GeoDetector model is based on the theory of geospatial heterogeneity. It can detect the spatial heterogeneity of land use and reveal the driving forces of LUCC by using factor detection and interaction detection, based on the interaction of single and double factors (Wang et al., 2010; Song et al., 2020). The specific expression is given by Equation 5. To explore the driving effect of each factor on LUCC, it is necessary to discretize the continuous factors. In this study, the natural discontinuity method was used to discretize the continuous factors.

$$q(x)=1-\frac{\sum_{k=1}^{K}N_{x,k}\sigma_{x,k}^2}{N_x\sigma_x^2}, \tag{5}$$

where $q(x)$ represents the value of driving forces of the influencing factor $x$ for the spatial distribution of LUCC; $N_x$ and $\sigma_x^2$ are the number and population variance of LUCC within the whole study area, respectively; and $N_{x,k}$ and $\sigma_{x,k}^2$ are the number and population variance of LUCC within the $k^{\mathrm{th}}$ ($k$=1, 2, …, $K$) subregion of factor $x$, respectively. The value range of $q(x)$ is from 0.00 to 1.00. The larger the value, the greater the impact of the influencing factor on the spatial heterogeneity of LUCC, and vice versa.

Interaction detection is the comparison of $q(x_1)$ and $q(x_2)$ with $q(x_1\cap x_2)$, which can be used to detect whether there is an enhancing or weakening effect of the two factors acting together. The types of interaction detection are listed in Table 2.

### 2.3.4 Data analysis

We used Origin, ArcMap 10.6, and Excel software to analyze the intensity and transition process

of LUCC. The $q$ value of each influencing factor on LUCC was calculated using GeoDetector (Wang et al., 2010; Song et al., 2020).

**Table 2** Description about the types of interaction detection

| Condition | Interaction |
|---|---|
| $q(x_1 \cap x_2) < \text{Min}(q(x_1), q(x_2))$ | Weaken, nonlinear |
| $\text{Min}(q(x_1), q(x_2)) < q(x_1 \cap x_2) < \text{Max}(q(x_1), q(x_2))$ | Weaken |
| $q(x_1 \cap x_2) > \text{Max}(q(x_1), q(x_2))$ | Enhance |
| $q(x_1 \cap x_2) = q(x_1) + q(x_2)$ | Independent |
| $q(x_1 \cap x_2) > q(x_1) + q(x_2)$ | Enhance, nonlinear |

Note: $x_1$ and $x_2$ represent the influencing factors; $q(x_1)$ and $q(x_2)$ represent the values of driving forces of $x_1$ and $x_2$ for the spatial distribution of LUCC, respectively; $q(x_1 \cap x_2)$ represents the value of driving forces of the interaction between $x_1$ and $x_2$; $\text{Min}(q(x_1), q(x_2))$ represents the minimum $q(x_1)$ and $q(x_2)$; $\text{Max}(q(x_1), q(x_2))$ represents the maximum $q(x_1)$ and $q(x_2)$.

## 3 Results

### 3.1 Spatiotemporal variation trajectory of LUCC

#### 3.1.1 Land-use structural change

The spatial distribution and area proportion of land-use types in the WRB from 1985 to 2020 are shown in Figure 2. In different periods, cultivated land has always been the major land-use type, and the area proportion consistently maintained at over 40.00%. The area proportions of forestland and grassland were both greater than 20.00% of the total study area. The sum of the areas of built-up land, bare land, and water body accounted for approximately 4.00% of the total area of the WRB. Additionally, the structure of LUCC evolved considerably during the study period, and the area proportion of each land-use type changed greatly before and after 2000. For example, cultivated land showed an increasing trend before 2000, whereas its area proportion decreased markedly from 46.81% to 44.33% after 2000. The growth rate of built-up land was slow before 2000 but it accelerated considerably after 2000. During the entire study period from 1985 to 2020, the areas of cultivated land, grassland, and bare land all exhibited decreasing trends, in which cultivated land decreased considerably from 62,466.50 to 59,673.51 km$^2$, with a reduction rate of approximately 4.50%. However, changes in grassland and bare land exhibited a slightly decreasing trend. Conversely, forestland, built-up land, and water body all increased to varying degrees from 1985 to 2020, with forestland increasing by 2593.92 km$^2$, built-up land by 3133.73 km$^2$, and water body by 80.08 km$^2$. Built-up land had the highest growth rate among all land-use types, with an average growth rate of 23.50%/5 a.

To explore the spatiotemporal heterogeneity of LUCC in the WRB, further analysis of LUCC evolution in each sub-basin is necessary. Figure 3 shows the characteristics of land-use types in each sub-basin over time. As shown in Figure 3, the spatial distribution of cultivated land was relatively even, with the MWRB and DWRB showing a marked decrease in the area proportion of cultivated land over time. The LRB and JRB were dominated by forestland and grassland, with the areas of forestland and grassland accounting for approximately 50.00% and 80.00% of the entire sub-basin, respectively. The area proportion of forestland and grassland in the JRB has increased since 2000. More than 90.00% of the built-up land area was distributed in the UWRB, MWRB, and DWRB. The area proportion of built-up land in the JRB and UWRB has increased over time. Bare land was concentrated in the LRB and JRB where human activities were less frequent, and there were opposing increasing and decreasing trends of the area proportion of bare land before and after 2000, respectively. Water body, in contrast to bare land, was concentrated in the middle and lower reaches of the main Weihe River, where human activities were more intensive; before 2000, the area of water body in the UWRB, MWRB, and DWRB accounted for more than 90.00% of the total water body in the WRB. However, after 2000, the area proportion of water body in the LRB, JRB, and UWRB showed an increasing trend.

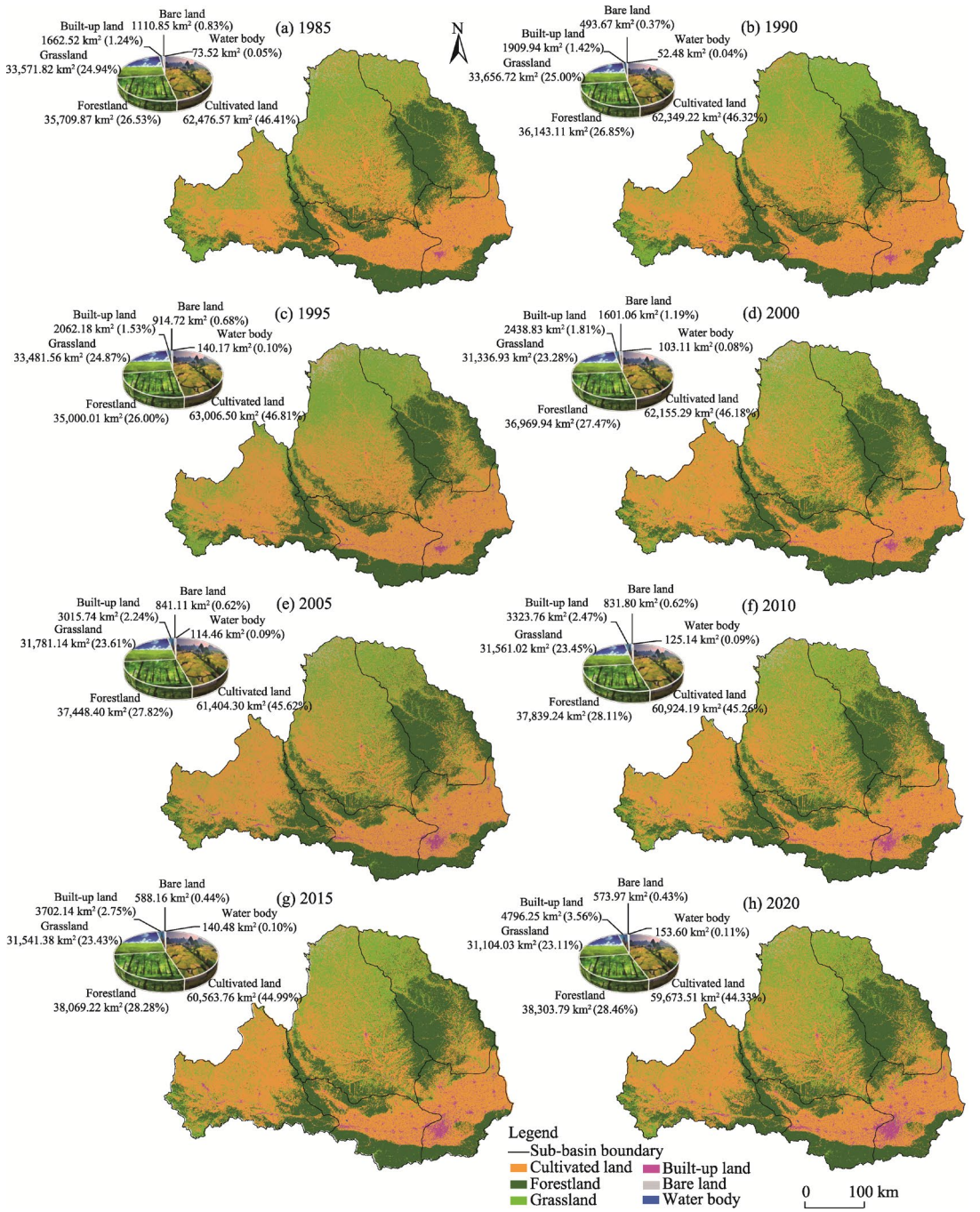


**Fig. 2** Spatial distribution and area proportions of land-use types in the WRB in 1985 (a), 1990 (b), 1995 (c), 2000 (d), 2005 (e), 2010 (f), 2015 (g), and 2020 (h)

### 3.1.2 Land-use transfer characteristics

Land-use structure change can show the variation in the overall pattern at the macroscopic level, but it cannot express the change in the rate of each land-use type. To further determine the transfer changes between land-use types in the WRB, we analyzed the dynamic transfer values of land-use types in each period, as shown in Figure 4 and Table S1 (in supplementary). The conversions among cultivated land, grassland, and forestland were the main features of land-use transfer in the WRB. Further, the transfers of the three land-use types were reversible. In

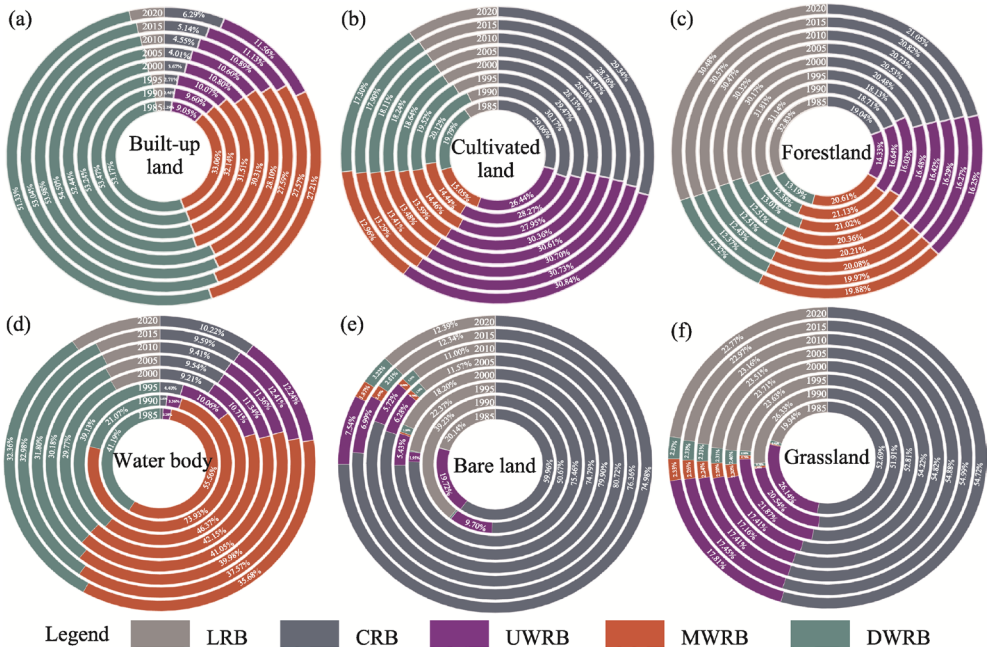


**Fig. 3** Area proportions of cultivated land (a), forestland (b), grassland (c), built-up land (d), bare land (e), and water body (f) in different sub-basins in the WRB from 1985 to 2020 at an interval of 5 a

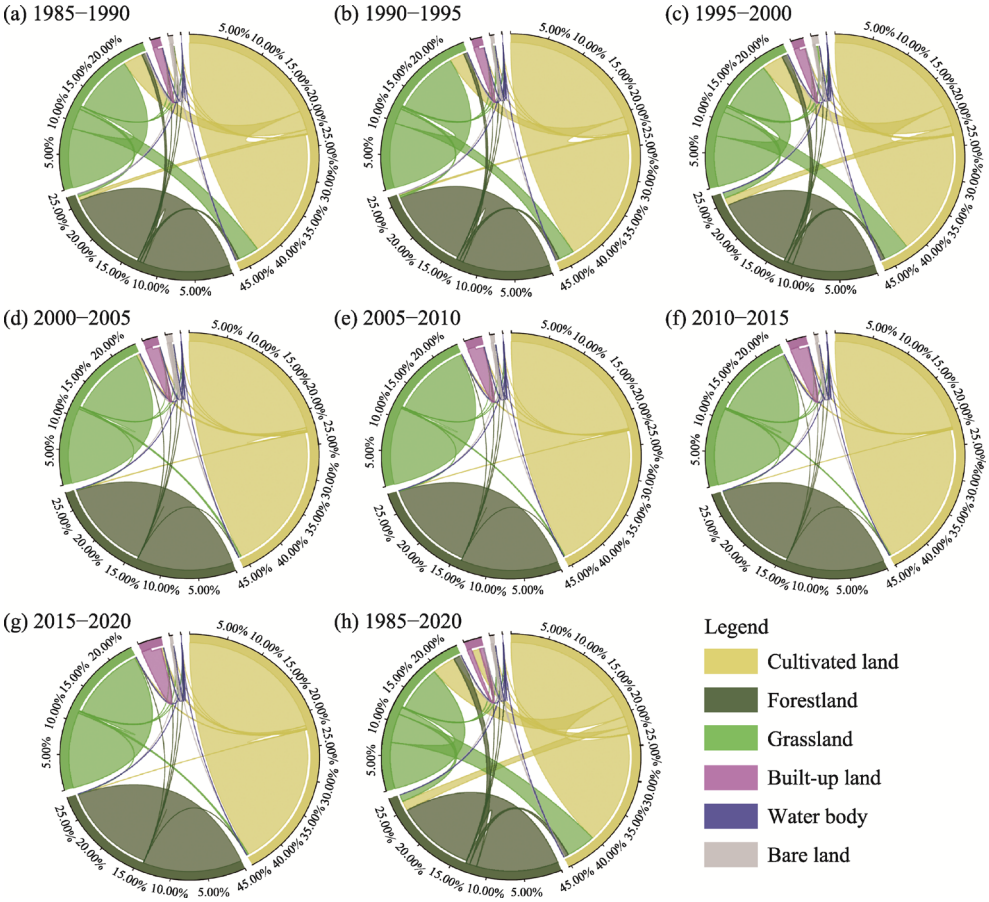


**Fig. 4** Structure chart of the transfers of different land-use types in the WRB in 1985–1990 (a), 1990–1995 (b), 1995–2000 (c), 2000–2005 (d), 2005–2010 (e), 2010–2015 (f), 2015–2020 (g), and 1985–2020 (h)

particular, the greatest proportion of mutual transfers among cultivated land, forestland, and grassland occurred before 2000. The sum of the area proportion of mutual transfers of the three land-use types reached 49.97%, 38.14%, and 66.83% in 1985–1990, 1990–1995, and 1995–2000, respectively. The increase in built-up land was mainly converted from cultivated land and grassland, among which cultivated land accounted for a large proportion. The area proportion of land converted from cultivated land to built-up land reached 64.71% in 1985–2020. It can be understood that the area proportion of cultivated land converted to built-up land increased dramatically since 2000. The proportions of water body and bare land areas were low. Moreover, the proportion of water body and bare land transfer did not exceed 1.50% in all periods.

To analyze the spatial characteristics of land-use conversion, we overlaid the land-use types spatially in each period and extracted the spatial change values of each land-use type. Given the small area of bare land and water body, the spatial characteristics these two land-use types were weakly represented. Figures 5 and 6 displayed only the spatial conversion results of major land-use types, including built-up land, cultivated land, forestland, and grassland.

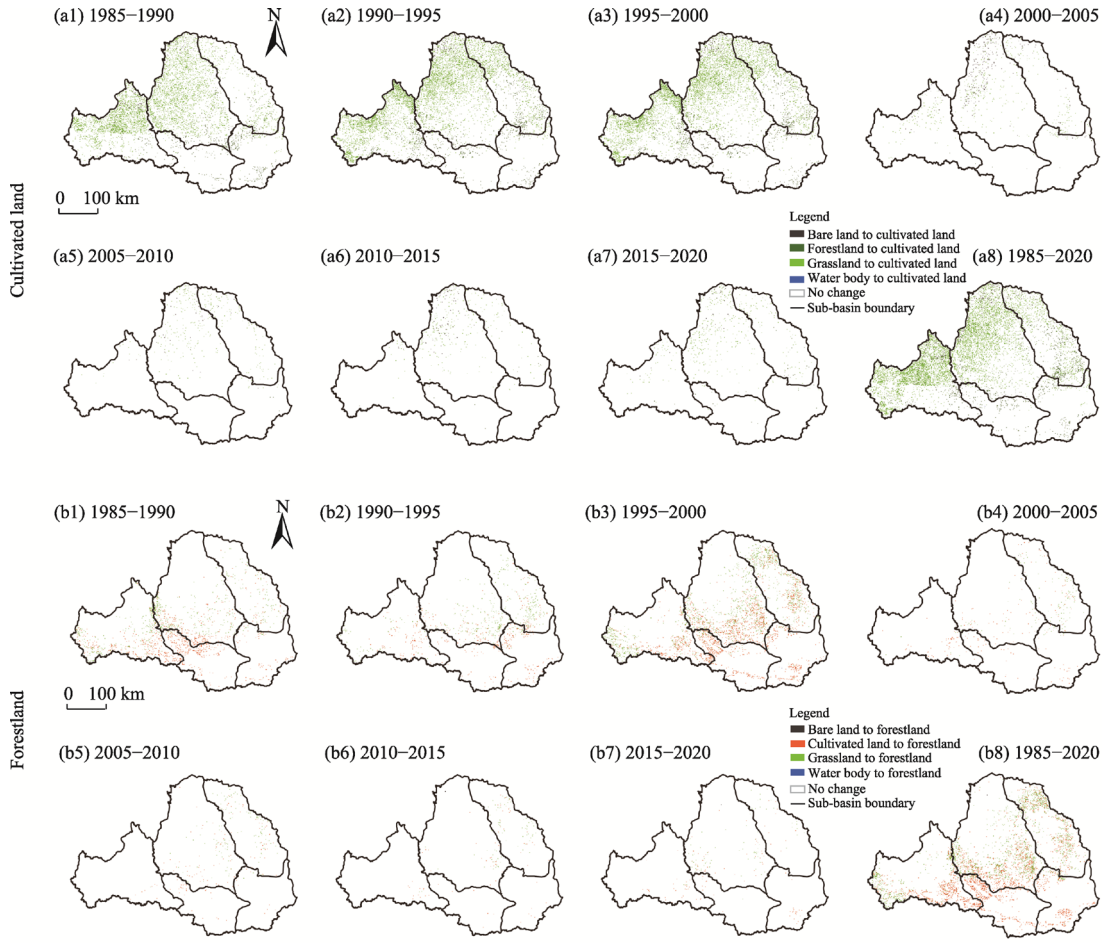


**Fig. 5** Spatial distribution of other land-use types converted to cultivated land (a1–a8) and forestland (b1–b8) in the WRB in 1985–1990 (a1 and b1), 1990–1995 (a2 and b2), 1995–2000 (a3 and b3), 2000–20005 (a4 and b4), 2005–2010 (a5 and b5), 2010–2015 (a6 and b6), 2015–2020 (a7 and b7), and 1985–2020 (a8 and b8)

As presented in Figures 5 and 6, complex conversions among cultivated land, forestland, and grassland were largely concentrated in the UWRB, JRB, and LRB, and the conversions were frequent before 2000. The interconversion between cultivated land and grassland was large and extensive, covering almost the majority of the WRB (Figs. 5a1–a8 and 6a1–a8). Forestland was

mainly converted to cultivated land and grassland, which were distributed in the middle and upper reaches of the WRB. In 1995–2000, the conversion of forestland was more dramatic and the area increased considerably, mainly from the conversion of cultivated land and grassland in the LRB (Fig. 5b1–b8). In contrast, the area of built-up land has been growing and was mainly concentrated in the plains of the UWRB, MWRB, and DWRB. The area of built-up land increased at the fastest rate in the DWRB, indicating that it was more influenced by human activities. From 1985 to 2020, built-up land increased in all sub-basins, and it was mainly converted from cultivated land and concentrated near the rivers. This could affect the hydrological cycle of the WRB.

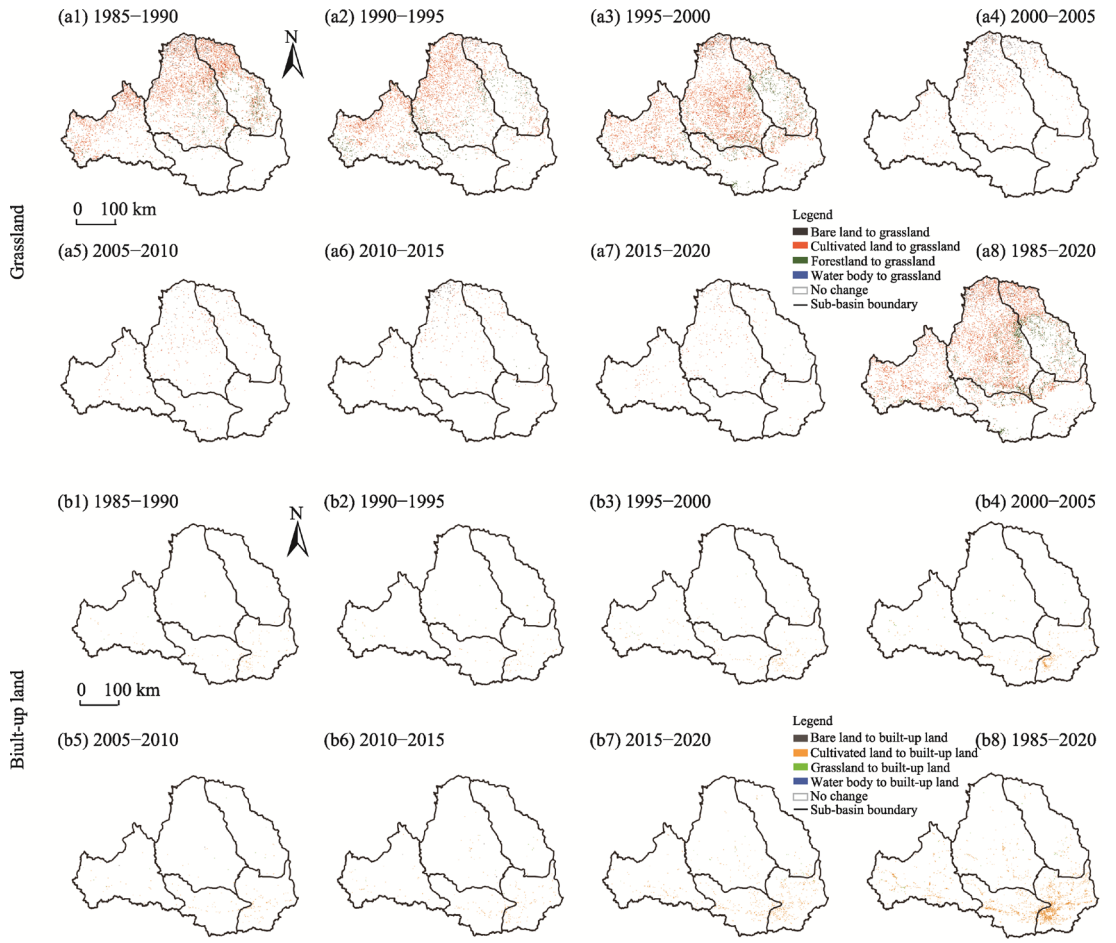


**Fig. 6** Spatial distribution of other land-use types converted to grassland (a1–a8) and built-up land (b1–b8) in the WRB in 1985–1990 (a1 and b1), 1990–1995 (a2 and b2), 1995–2000 (a3 and b3), 2000–20005 (a4 and b4), 2005–2010 (a5 and b5), 2010–2015 (a6 and b6), 2015–2020 (a7 and b7), and 1985–2020 (a8 and b8)

### 3.1.3 Dynamic change in land use

Both comprehensive land-use dynamic index and single land-use dynamic index (including relative land-use dynamic index and absolute land-use dynamic index) were calculated to further analyze the intensity and rate of change in land use. During the study period, the comprehensive land-use dynamic index first increased and later decreased (Table 3). The highest value of comprehensive land-use dynamic index occurred in 1990–1995, at 0.90%. After 2000, a high value of comprehensive land-use dynamic index (0.39%) was observed in 2015–2020. This indicates that land-use conversion was relatively drastic before 2000 and in 2015–2020.

The results of single land-use dynamic index for each land-use type are shown in Figure 7.

Bare land and water body had the highest relative land-use dynamic index and absolute land-use dynamic index values. This is because the basic area of bare land and water body was small; therefore, a small amount of land-use type area conversion can increase the relative dynamic change of land-use transfer.

**Table 3** Comprehensive land-use dynamic index in the Weihe River Basin (WRB) in 1985–2020 at an inverval of 5 a

| | 1985–1990 | 1990–1995 | 1995–2000 | 2000–2005 | 2005–2010 | 2010–2015 | 2015–2020 |
|---|---|---|---|---|---|---|---|
| Comprehensive land-use dynamic index (%) | 0.20 | 0.40 | 0.90 | 0.40 | 0.20 | 0.18 | 0.39 |

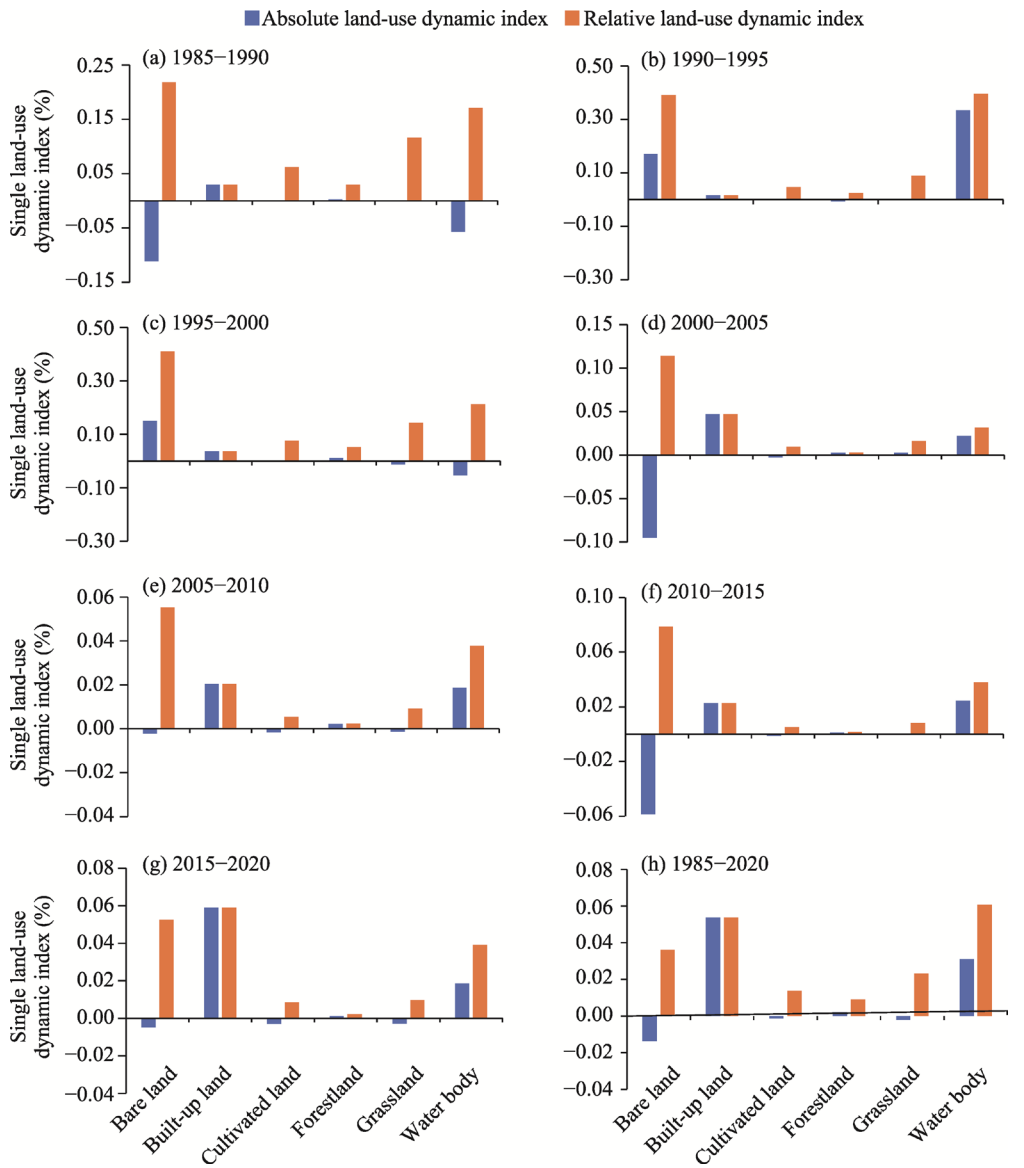


**Fig. 7** Single land-use dynamic index (including relative land-use dynamic index and absolute land-use dynamic index) values of land-use types in the WRB in 1985–1990 (a), 1990–1995 (b), 1995–2000 (c), 2000–2005 (d), 2005–2010 (e), 2010–2015 (f), 2015–2020 (g), and 1985–2020 (h). Note that values of relative or absolute land-use dynamic index less than zero represent decrease in the area of land-use type, and values of relative or absolute land-use dynamic index greater than zero represent increase in the area of land-use type.

Before 2000, the relative land-use dynamic index values of changes in cultivated land, forestland, and grassland were far higher than those after 2000. This indicates that these three land-use types were converted more actively before 2000. The relative land-use dynamic index and absolute land-use dynamic index of built-up land remained consistent, which was the result that built-up land has not been converted to other land-use types. The single dynamic index of built-up land was positive, with an increase after 2000. It can also be seen that the dramatic comprehensive land-use dynamic index in 2015–2020 was the result of an increase in built-up land. Throughout the study period (Fig. 7h), all land-use types were found to be active in interconversion, as evidenced by the relative land-use dynamic index. Areas of built-up land, water body, and forestland showed positive increases (absolute land-use dynamic index higher than zero) during the study period, whereas areas of cultivated land, grassland, and bare land all exhibited varying degrees of decrease (absolute land-use dynamic index lower than zero).

## 3.2 Driving factor detection of LUCC

### 3.2.1 Single factor detector of LUCC

Based on the selected influencing factors, we detected the driving forces of LUCC in the WRB and each sub-basin from 1985 to 2020 using the GeoDetector. The changes in the $q$ value of each influencing factor in the WRB and its sub-basins are shown in Figure 8, presenting different driving effects for different periods in different sub-basins. The factors showed strong driving forces for LUCC before 2000, which was related to the high dynamic change in LUCC before 2000. However, in the DWRB, the $q$ values of population density and GDP on LUCC gradually increased after 2000, indicating that LUCC was influenced by human activities. This finding was consistent with above-mentioned observed trends in LUCC, with a shift towards built-up land across all land-use types.

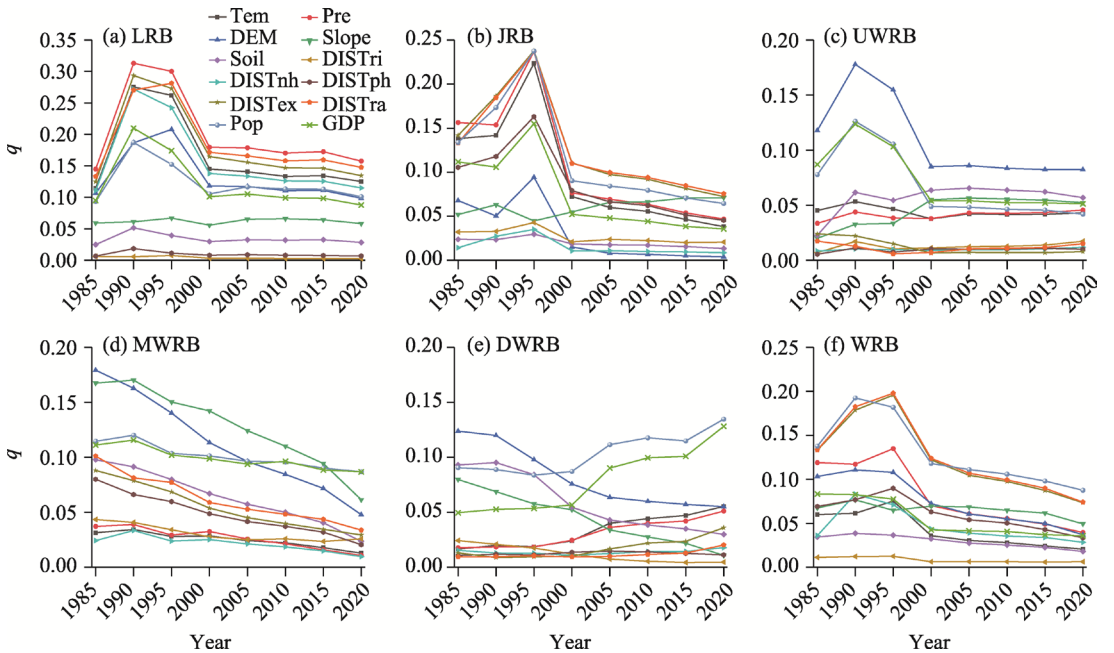


**Fig. 8** Variations of $q$ values for different influencing factors of LUCC in the WRB and its sub-basins from 1985 to 2020. (a), LRB; (b), JRB; (c), UWRB; (d), MWRB; (e), DWRB; (f), WRB. $q$, the value of driving forces of the influencing factor; Tem, temperature; Pre, precipitation; DEM, elevation; DISTri, distance to rivers; DISTnh, distance to national highway; DISTph, distance to provincial highway; DISTex, distance to expressway; DISTra, distance to railway; Pop, population density; GDP, gross domestic product.

According to the 5-a average driving forces (Fig. 9), the major influencing factors of LUCC varied considerably among the sub-basins. The WRB was influenced by population density, distance to railway, and distance to expressway, which are closely related to human activities,

followed by precipitation, DEM, and slope, which are correlated with topography and geographical location. Among the sub-basins, the LRB and JRB were more similar and mostly driven by precipitation and temperature, which are related to the large area of forestland and grassland of these two sub-basins. Distance to railway and distance to expressway also had greater influences on LUCC in these two sub-basins. The LUCC of the UWRB, MWRB, and DWRB was considerably driven by topography (DEM and slope) and human activities (population density and GDP). This may be related to the geographical location of these three sub-basins, and human activities played a vital role in the conversion of built-up land.

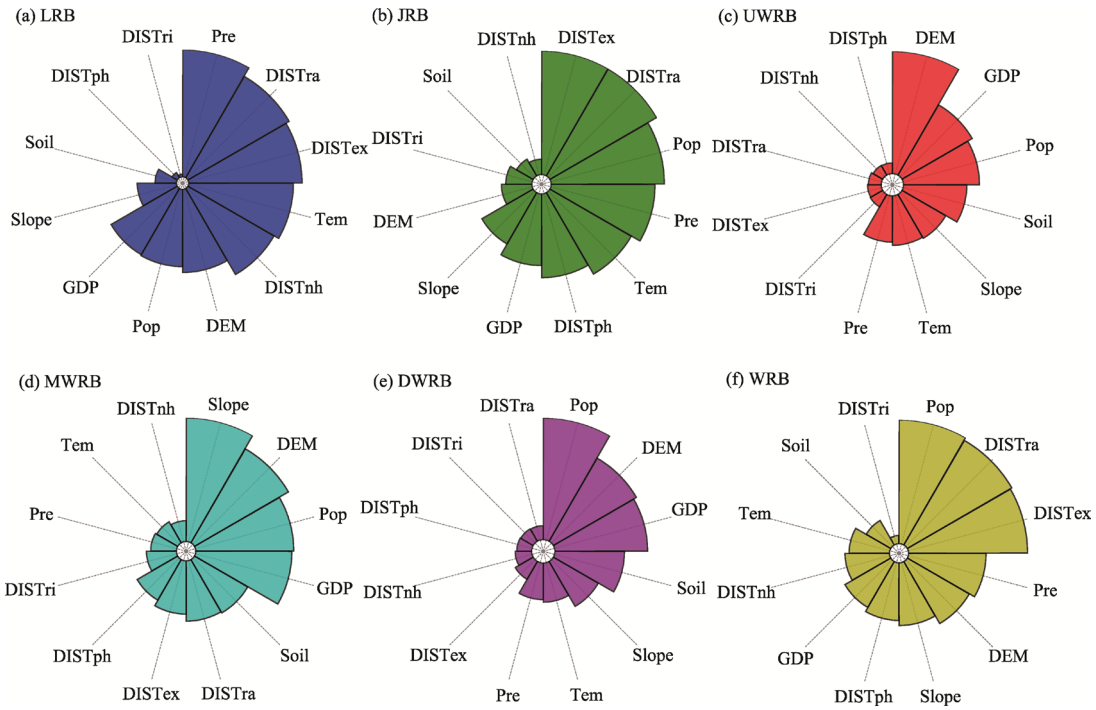


**Fig. 9** Average *q* value of each influencing factor of LUCC in the WRB and its sub-basins. (a), LRB; (b), JRB; (c), UWRB; (d), MWRB; (e), DWRB; (f), WRB. *q*, the value of driving forces of the influencing factor; Tem, temperature; Pre, precipitation; DEM, elevation; DISTri, distance to rivers; DISTnh, distance to national highway; DISTph, distance to provincial highway; DISTex, distance to expressway; DISTra, distance to railway; Pop, population density; GDP, gross domestic product.

### 3.2.2 Factor interaction detection of LUCC

The results of the 5-a average interaction of influencing factors of LUCC in the WRB and its sub-basins are shown in Figure 10. The spatial distribution of LUCC in the WRB was strongly affected by the interactions of meteorological factors, natural factors, social factors, and human activity factors, with the interaction factors in each sub-basin showing a linear or non-linear enhancement effect. LUCC in the WRB was mainly affected by the large interaction of population density∩temperature, population density∩precipitation, and population density∩slope. The UWRB was subject to a stronger interaction of DEM with meteorological factors ($q$=1.35) than DEM with human activity factors ($q$ values of 0.94–1.14), followed by a stronger interaction of meteorological factors with human activity factors. Both the MWRB and DWRB were affected by the interaction of topography factors and human activity factors considerably, with $q$(population density∩slope)=1.61 and $q$(GDP∩slope)=1.61 in the MWRB, and $q$(population density∩DEM)=1.44 and $q$(GDP∩DEM)=1.37 in the DWRB. The JRB was considerably affected by the interaction of social factors and slope. The interaction of all influencing factors in the LRB was stronger, which is related to the greater driving forces of individual influencing factors. This also indicates that LUCC in the LRB was more susceptible to change.

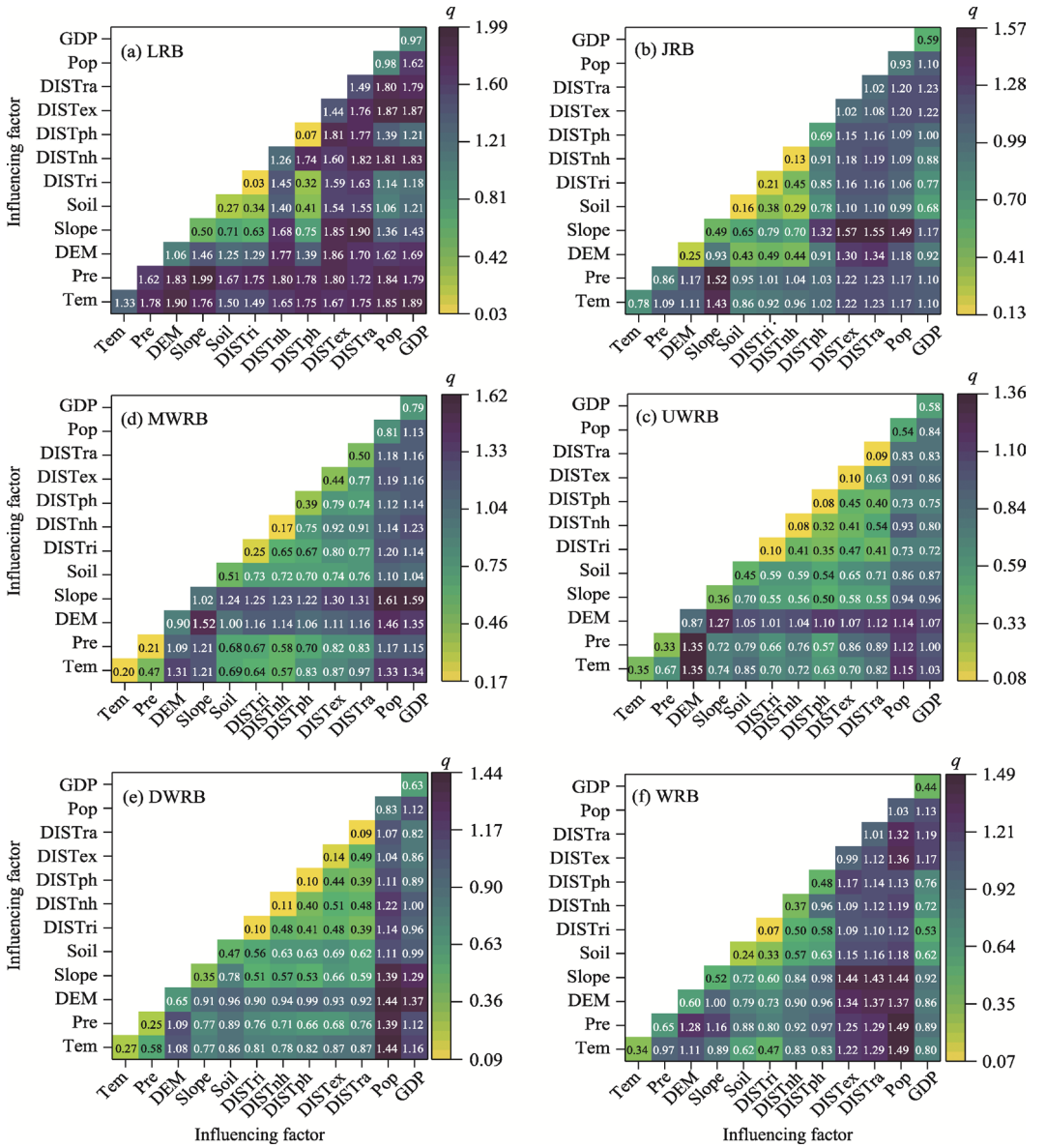


**Fig. 10** Heat map of the 5-a average interaction of influencing factors of LUCC in the WRB and its sub-basins from 1985 to 2020. (a), LRB; (b), JRB; (c), UWRB; (d), MWRB; (e), DWRB; (f), WRB. Tem, temperature; Pre, precipitation; DEM, elevation; DISTri, distance to rivers; DISTnh, distance to national highway; DISTph, distance to provincial highway; DISTex, distance to expressway; DISTra, distance to railway; Pop, population density; GDP, gross domestic product.

## 4 Discussion

### 4.1 Spatiotemporal differences of LUCC driven by policies

In the WRB, LUCC exhibited spatiotemporal heterogeneity, with separate responses to each sub-basin. This phenomenon is influenced by the difference in the spatial distribution patterns of land-use types and the implementation of various projects (Jian et al., 2015; Xu et al., 2022). Artificial landscapes (e.g., cultivated land and built-up land) responded the most remarkably to the implementation of projects. The area of cultivated land had a substantial growth trend before 2000, however, with the formal launch of the Grain for Green Project in 1999 (Jian et al., 2015; Wang et al., 2017), the area of cultivated land gradually decreased after 2000. The purpose of the

Grain for Green Project is to restore forest vegetation and improve the damaged eco-environment by stopping reclaiming cultivated land that is unsuitable for cultivation and is prone to soil erosion. With the implementation of this project, a large amount of cultivated land has been converted to forestland, resulting in an increasing in the area of forestland. Additionally, the results of spatial conversion of land-use types showed that the conversions among cultivated land, forestland, and grassland were concentrated in the JRB, LRB, and UWRB (Figs. 5 and 6). This was related to the large area of these three land-use types in the JRB, LRB, and UWRB, and may also because the Loess Plateau is one of the early pilots of the Grain for Green Project (Xu et al., 2022).

During the entire study period (1985–2020), the area of built-up land has always maintained a growth trend and has accelerated after 2000 (Wu et al., 2021), which responded to the 'Urbanization Special Plan' issued by the National Planning Commission (National Development and Reform Commission since 2003) in 2001 (Wu et al., 2021; Huang et al., 2022). The implementation of this plan has accelerated the urbanization process, causing a rapid increase in the area of built-up land. The increase of built-up land area was concentrated in the MWRB and DWRB. The conversion of other land-use types to built-up land was dramatic in 2015–2020 (Fig. 6; Table 3), which was related to the rapid development of Xi'an, Baoji, and Weinan, i.e., the major cities of Shaanxi Province. The expansion of built-up land can only cope with the rapid development of society and economy, and the expansion of built-up land resulting from this development will not change. Additionally, the implementation of the Grain for Green Project and soil and water conservation and environmental protection measures, has improved the eco-environment of the WRB and increased the area of water body (Jian et al., 2015; Zhou et al., 2016).

The results of the dynamic change of land uses in the WRB in each period from 1985 to 2020 further confirmed the rapid improvement in land-use development driven by relevant national policies. However, geographical location and socioeconomic conditions can lead to uneven land-use development in each sub-basin. Consequently, it is necessary to formulate targeted differentiation management models to achieve the sustainable development of the whole basin based on the full consideration of the regional variations in LUCC.

### 4.2 Distribution patterns of LUCC driven by influencing factors

LUCC in the WRB was influenced by population density, distance to railway, and distance to expressway (Fig. 9). Distance to railway and distance to expressway are closely related to the subsidiary infrastructure of the human pursuit of rapid development (Ma and Xu, 2010). Therefore, human activities play a major driving role in LUCC in the WRB, which is closely related to population growth and urbanization (Ma and Xu, 2010; Wu et al., 2021; Yuan et al., 2022). This also explains the rapid growth and relatively high dynamic changes in built-up land in the WRB.

However, the results of this study showed varying driving effects of each influencing factor on LUCC in each sub-basin (Fig. 11). LUCC in the LRB and JRB was driven by the meteorological factors (precipitation and temperature) and social factors (distance to railway and distance to expressway), which were closely related to the relatively large shares of forestland and grassland in these two sub-basins. Large areas of the LRB and JRB are situated on the Loess Plateau with limited precipitation. Therefore, changes in precipitation and temperature are more sensitive to the growth of forestland and grassland (Nie et al., 2021). A higher road network density also tends to cause the landscape fragmentation of forestland and grassland, with more severe impacts on ecologically fragile areas (Xu et al., 2022; Yuan et al., 2022). LUCC in the UWRB, MWRB, and DWRB was mainly influenced by the natural factors (DEM and slope) and human activity factors (population density and GDP). The primary reason was that cultivated land and built-up land were the main land-use types in these three sub-basins. Slope and DEM were the major factors affecting the distribution of cultivated land and the expansion of built-up land in the WRB (Wu et al., 2021; Wei et al., 2022).

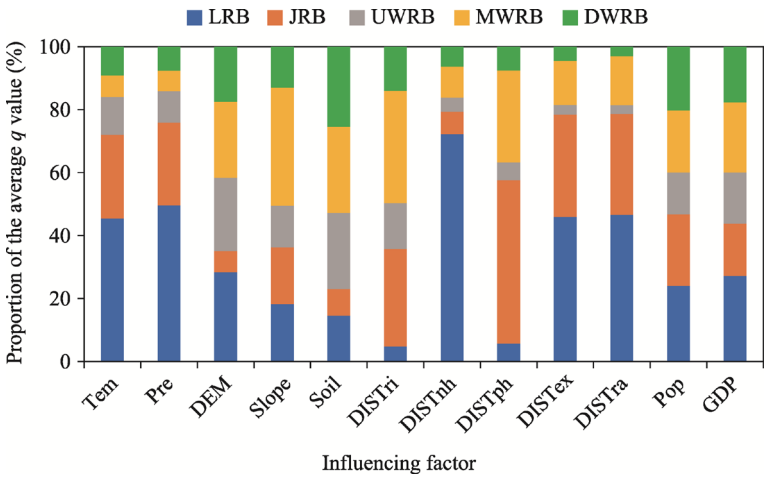


**Fig. 11** Proportion of the average $q$ value of each influencing factor of LUCC in each sub-basin of the WRB. $q$, the value of driving forces of the influencing factor; Tem, temperature; Pre, precipitation; DEM, elevation; DISTri, distance to rivers; DISTnh, distance to national highway; DISTph, distance to provincial highway; DISTex, distance to expressway; DISTra, distance to railway; Pop, population density; GDP, gross domestic product.

The formation and evolution of the spatial patterns of land-use types in the WRB are subject to a combination of natural geography, socioeconomic factors, and policy planning (Wang et al., 2017; Wu et al., 2021; Huang et al., 2022). Because policy planning is difficult to quantify, this study only conducted a qualitative analysis. The interaction of natural geography and socioeconomic factors showed linear or nonlinear enhancement, where the interaction of human activity factors with other factors always showed a strong driving effect on LUCC in the WRB. According to the obtained results of the driving force interactions (Fig. 10), human activity factors∩social factors, human activity factors∩natural factors, and human activity factors∩meteorological factors also showed high driving forces on LUCC in each sub-basin. This was closely related to human activities, such as deforestation, overgrazing, bare land reclamation, and built-up activities (Bai et al., 2019; Yang, 2021). As a result, the interaction of human activity factors with other factors dominated the main cause of LUCC across the basin.

However, there was also spatial heterogeneity in the interaction of the influencing factors of LUCC across the sub-basins. The interaction between social factors and natural factors also had relatively high effects on LUCC in the UWRB and MWRB. This indicates that socioeconomic development is closely related to the natural environment (Chen et al., 2016; Wei et al., 2021). The interactions of the influencing factors in the LRB and JRB were substantially greater than those in the other three sub-basins. This implies that the LRB and JRB are more complex and driven by multiple factors, and any change in influencing factors may have a great impact on LUCC. This also confirmes the ecological vulnerability of the LRB and JRB (Nie et al., 2021; Xu et al., 2022).

## 5 Conclusions

Using land-use data of the WRB from 1985 to 2020, this study analyzed the driving forces behind the spatiotemporal heterogeneity of LUCC in this region. The driving forces of the influencing factors of LUCC in the WRB and its sub-basins were quantified and analyzed. LUCC in the WRB showed the largest area proportion of cultivated land, followed by forestland and grassland. The dynamic transfer of LUCC fluctuated dramatically before and after the year 2000. The conversion rate among cultivated land, forestland, and grassland was high before 2000, which was mainly influenced by the implementation of various projects, and the conversion was primarily concentrated in the LRB, JRB, and UWRB. The area of built-up land increased remarkably after

2000 due to socioeconomic development in the UWRB, MWRB, and DWRB. LUCC in the WRB was driven by multiple influencing factors and the driving role varied across different sub-basins. The LRB and JRB were highly driven by the meteorological factors and social factors, and were sensitive to the interaction of the influencing factors. The UWRB, MWRB, and DWRB were driven by the human activity factors and natural factors, which also dominated the factor-driven characteristics of LUCC in the entire WRB.

Land-use management policies should be formulated according to local conditions, and coordination between natural environment and socioeconomic factors should be emphasized in future development. In land-use management, zoning control strategies should be formulated by considering the spatiotemporal heterogeneity of LUCC in each sub-basin and its driving mechanisms. In the LRB and JRB that are influenced by the meteorological factors and social factors, attention should be paid to the effects of changes in the climate and environment. Ecological and environmental protection needs to be strengthened in areas disturbed by the construction of roads and railroads. The future socioeconomic development in the UWRB, MWRB, and DWRB that are subject to intensive human activities should focus on the coordinated development of nature-society-economy-ecology to achieve the sustainable development of the basin.



## Acknowledgements

This study was supported by the Natural Science Basic Research Program of Shaanxi Province (2019JLZ-15), the Water Science and Technology Program of Shaanxi Province (2018slkj-4), and the Research Fund of the State Key Laboratory of Eco-hydraulics in Northwest Arid Region, Xi'an University of Technology (2019KJCXTD-5). The authors are grateful to the editors and anonymous reviewers for their insightful comments and suggestions.

## References

Bai L M, Xiu C L, Feng X H, et al. 2019. Influence of urbanization on regional habitat quality: a case study of Changchun City. Habitat International, 93: 102042, doi: 10.1016/j.habitatint.2019.102042.

Batunacun, Nendel C, Hu Y F, et al. 2018. Land-use change and land degradation on the Mongolian Plateau from 1975 to 2015—A case study from Xilingol, China. Land Degradation & Development, 29(6): 1595–1606.

Chen M X, Li Y, Gong Y H, et al. 2016. The population distribution and trend of urbanization pattern on two sides of Hu Huanyong population line: A tentative response to Premier Li Keqiang. Acta Geographica Sinica, 71(2): 179–193. (in Chinese)

Du J, Shi C X. 2012. Effects of climatic factors and human activities on runoff of the Weihe River in recent decades. Quaternary International, 282: 58–65.

Guo B, Wang Y, Pei L, et al. 2021. Determining the effects of socioeconomic and environmental determinants on chronic obstructive pulmonary disease (COPD) mortality using geographically and temporally weighted regression model across Xi'an during 2014–2016. Science of The Total Environment, 756: 143869, doi: 10.1016/j.scitotenv.2020.143869.

Hasselmann F, Csaplovics E, Falconer I, et al. 2010. Technological driving forces of LUCC: Conceptualization, quantification, and the example of urban power distribution networks. Land Use Policy, 27(2): 628–637.

Huang X X, Wang H J, Xiao F T. 2022. Simulating urban growth affected by national and regional land use policies: Case study from Wuhan, China. Land Use Policy, 112: 105850, doi: 10.1016/j.landusepol.2021.105850.

Jian S Q, Zhao C Y, Fang S M, et al. 2015. Effects of different vegetation restoration on soil water storage and water balance in the Chinese Loess Plateau. Agricultural and Forest Meteorology, 206: 85–96.

Jiang L, Yu J, Wen J H, et al. 2021. Risk assessment of extreme flood in the north bank of the Hangzhou Bay under land use change scenarios. Progress in Geography, 40(8): 1355–1370. (in Chinese)

Kindu M, Angelova D, Schneider T, et al. 2020. Monitoring of urban growth patterns in rapidly growing Bahir Dar City of northwest Ethiopia with 30 year Landsat imagery record. ISPRS International Journal of Geo-Information, 9(9): 548, doi: 10.3390/ijgi9090548.

Kong X S, Fu M X, Zhao X, et al. 2022. Ecological effects of land-use change on two sides of the Hu Huanyong Line in China. Land Use Policy, 113: 105895, doi: 10.1016/j.landusepol.2021.105895.

Ma Y L, Xu R S. 2010. Remote sensing monitoring and driving force analysis of urban expansion in Guangzhou City, China. Habitat International, 34(2): 228–235.

Nhi P T T, Khoi D N, Trang N T T, et al. 2022. Hydrological impacts of future climate and land use/cover changes in the Lower Mekong Basin: a case study of the Srepok River Basin, Vietnam. Environmental Monitoring and Assessment, 194(Suppl 2): 768, doi: 10.1007/s10661-022-10175-9.

Nie T, Dong G T, Jiang X H, et al. 2021. Spatio-temporal changes and driving forces of vegetation coverage on the Loess Plateau of northern Shaanxi. Remote Sensing, 13(4): 613, doi: 10.3390/rs13040613.

Ning J, Liu J Y, Kuang W H, et al. 2018. Spatiotemporal patterns and characteristics of land-use change in China during 2010–2015. Journal of Geographical Sciences, 28(5): 547–562.

Omer A, Ma Z G, Yuan X, et al. 2021. A hydrological perspective on drought risk-assessment in the Yellow River Basin under future anthropogenic activities. Journal of Environmental Management, 289: 112429, doi: 10.1016/j.jenvman.2021.112429.

Shaharum N S N, Shafri H Z M, Gambo J, et al. 2018. Mapping of Krau Wildlife Reserve (KWR) protected area using Landsat 8 and supervised classification algorithms. Remote Sensing Applications: Society and Environment, 10: 24–35.

Song F, Su F L, Mi C X, et al. 2021. Analysis of driving forces on wetland ecosystem services value change: A case in Northeast China. Science of The Total Environment, 751: 141778, doi: 10.1016/j.scitotenv.2020.141778.

Song Y Z, Wang J F, Ge Y, et al. 2020. An optimal parameters-based geographical detector model enhances geographic characteristics of explanatory variables for spatial heterogeneity analysis: cases with different types of spatial data. GIScience & Remote Sensing, 57(5): 593–610.

Sun X, Lu Z M, Li F, et al. 2018. Analyzing spatio-temporal changes and trade-offs to support the supply of multiple ecosystem services in Beijing, China. Ecological Indicators, 94: 117–129.

Wang H Y, Qin F, Xu C D, et al. 2021. Evaluating the suitability of urban development land with a Geodetector. Ecological Indicators, 123: 107339, doi: 10.1016/j.ecolind.2021.107339.

Wang J F, Li X H, Christakos G, et al. 2010. Geographical detectors-based health risk assessment and its application in the neural tube defects study of the Heshun Region, China. International Journal of Geographical Information Science, 24(1): 107–127.

Wang J T, Peng J, Zhao M Y, et al. 2017. Significant trade-off for the impact of Grain-for-Green Programme on ecosystem services in North-western Yunnan, China. Science of The Total Environment, 574: 57–64.

Wei H, Xiong L Y, Tang G A, et al. 2021. Spatial-temporal variation of land use and land cover change in the glacial affected area of the Tianshan Mountains. CATENA, 202: 105256, doi: 10.1016/j.catena.2021.105256.

Wei X D, Lin L G, Luo P P, et al. 2022. Spatiotemporal pattern and driving force analysis of multi-functional coupling coordinated development of cultivated land. Transactions of the Chinese Society of Agricultural Engineering, 38(4): 260–269. (in Chinese)

Wu J Y, Luo J G, Zhang H, et al. 2022a. Projections of land use change and habitat quality assessment by coupling climate change and development patterns. Science of The Total Environment, 847: 157491, doi: 10.1016/ j.scitotenv.2022.157491.

Wu J Y, Luo J G, Du X Z, et al. 2022b. Optimizing water allocation in an inter-basin water diversion project with equity-efficiency tradeoff: A bi-level multiobjective programming model under uncertainty. Journal of Cleaner Production, 371: 133606, doi: 10.1016/j.jclepro.2022.133606.

Wu R, Li Z G, Wang S J, 2021. The varying driving forces of urban land expansion in China: Insights from a spatial-temporal analysis. Science of The Total Environment, 766: 142591, doi: 10.1016/j.scitotenv.2020.142591.

Wulder M A, White J C, Goward S N, et al. 2008. Landsat continuity: Issues and opportunities for land cover monitoring. Remote Sensing of Environment, 112(3): 955–969.

Xu C, Jiang Y N, Su Z H, et al. 2022. Assessing the impacts of Grain-for-Green Programme on ecosystem services in Jinghe River basin, China. Ecological Indicators, 137: 108757, doi: 10.1016/j.ecolind.2022.108757.

Yang C, Wei T X, Li Y R, 2022. Simulation and spatio-temporal variation characteristics of LULC in the context of urbanization construction and ecological restoration in the Yellow River Basin. Sustainability, 14(2): 789, doi: 10.3390/su14020789.

Yang Y Y. 2021. Evolution of habitat quality and association with land-use changes in mountainous areas: A case study of the Taihang Mountains in Hebei Province, China. Ecological Indicators, 129: 107967, doi: 10.1016/j.ecolind.2021.107967.

Yuan Z F, Zhou L, Sun D Q, et al. 2022. Impacts of urban expansion on the loss and fragmentation of cropland in the major grain production areas of China. Land, 11(1): 130, doi: 10.3390/land11010130.

Zhan Q Q, Zhao W, Yang M J, et al. 2021. A long-term record (1995–2019) of the dynamics of land desertification in the middle reaches of Yarlung Zangbo River basin derived from Landsat data. Geography and Sustainability, 2(1): 12–21.

Zhang X, Liu L Y, Chen X D, et al. 2021. GLC_FCS30: Global land-cover product with fine classification system at 30 m using time-series Landsat imagery. Earth System Science Data, 13(6): 2753–2776.

Zhou J, Fu B J, Gao G Y, et al. 2016. Effects of precipitation and restoration vegetation on soil erosion in a semi-arid environment in the Loess Plateau, China. CATENA, 137: 1–11.

Zhou L, Dang X W, Sun Q K, et al. 2020. Multi-scenario simulation of urban land change in Shanghai by random forest and CA-Markov model. Sustainable Cities and Society, 55: 102045, doi: 10.1016/j.scs.2020.102045.

## Appendix

**Table S1** Transfer matrix of land-use and land-cover change (LUCC) in different periods (unit: $km^2$)

| Period | | Bare land | Built-up land | Cultivated land | Forestland | Grassland | Water body | Total |
|---|---|---|---|---|---|---|---|---|
| | Bare land | 195.75 | 0.26 | 217.75 | 0.01 | 697.08 | 0.00 | 1110.85 |
| | Built-up land | 0.00 | 1662.52 | 0.00 | 0.00 | 0.00 | 0.00 | 1662.52 |
| | Cultivated land | 123.60 | 239.19 | 52,719.58 | 1658.10 | 7723.83 | 12.26 | 62,476.57 |
| 1985–1990 | Forestland | 0.05 | 0.72 | 1057.96 | 33,275.83 | 1366.82 | 8.49 | 35,709.87 |
| | Grassland | 174.28 | 7.21 | 8313.03 | 1208.17 | 23,868.92 | 0.21 | 33,571.82 |
| | Water body | 0.00 | 0.05 | 40.90 | 0.99 | 0.07 | 31.52 | 73.52 |
| | Total | 493.67 | 1909.94 | 62,349.22 | 36,143.11 | 33,656.72 | 52.48 | 134,605.14 |
| Period | | Bare land | Built-up land | Cultivated land | Forestland | Grassland | Water body | Total |
| | Bare land | 222.72 | 0.22 | 80.13 | 0.00 | 190.44 | 0.16 | 493.67 |
| | Built-up land | 0.00 | 1909.94 | 0.00 | 0.00 | 0.00 | 0.00 | 1909.94 |
| | Cultivated land | 130.40 | 141.41 | 55,346.24 | 780.44 | 5858.73 | 91.99 | 62,349.22 |
| 1990–1995 | Forestland | 0.00 | 0.03 | 1362.27 | 33,410.33 | 1367.65 | 2.83 | 36,143.11 |
| | Grassland | 561.60 | 10.52 | 6211.72 | 808.50 | 26,063.58 | 0.80 | 33,656.72 |
| | Water body | 0.00 | 0.07 | 6.14 | 0.73 | 1.15 | 44.40 | 52.48 |
| | Total | 914.72 | 2062.18 | 63,006.50 | 35,000.01 | 33,481.56 | 140.17 | 134,605.14 |
| Period | | Bare land | Built-up land | Cultivated land | Forestland | Grassland | Water body | Total |
| | Bare land | 321.44 | 0.65 | 217.20 | 3.69 | 371.01 | 0.74 | 914.72 |
| | Built-up land | 0.00 | 2062.18 | 0.00 | 0.00 | 0.00 | 0.00 | 2062.18 |
| | Cultivated land | 429.78 | 356.81 | 50,557.45 | 3187.17 | 8430.70 | 44.59 | 63,006.50 |
| 1995–2000 | Forestland | 1.84 | 0.16 | 1448.02 | 31,426.82 | 2121.59 | 1.58 | 35,000.01 |
| | Grassland | 843.62 | 18.22 | 9856.08 | 2349.17 | 20,405.21 | 9.27 | 33,481.56 |
| | Water body | 4.38 | 0.80 | 76.55 | 3.09 | 8.42 | 46.93 | 140.17 |
| | Total | 1601.06 | 2438.83 | 62,155.29 | 36,969.94 | 31,336.93 | 103.11 | 134,605.14 |
| Period | | Bare land | Built-up land | Cultivated land | Forestland | Grassland | Water body | Total |
| | Bare land | 764.48 | 3.56 | 330.92 | 6.68 | 495.06 | 0.36 | 1601.06 |
| | Built-up land | 0.00 | 2438.83 | 0.00 | 0.00 | 0.00 | 0.00 | 2438.83 |
| | Cultivated land | 40.82 | 543.03 | 60,262.11 | 305.95 | 991.16 | 12.23 | 62,155.29 |
| 2000–2005 | Forestland | 0.02 | 2.97 | 28.63 | 36,920.91 | 17.18 | 0.23 | 36,969.94 |
| | Grassland | 35.69 | 27.33 | 780.64 | 214.70 | 30,277.49 | 1.07 | 31,336.93 |
| | Water body | 0.10 | 0.03 | 2.00 | 0.16 | 0.25 | 100.57 | 103.11 |
| | Total | 841.11 | 3015.74 | 61,404.30 | 37,448.40 | 31,781.14 | 114.46 | 134,605.14 |
| Period | | Bare land | Built-up land | Cultivated land | Forestland | Grassland | Water body | Total |
| | Bare land | 720.35 | 3.50 | 56.27 | 1.02 | 59.91 | 0.07 | 841.11 |
| | Built-up land | 0.00 | 3015.74 | 0.00 | 0.00 | 0.00 | 0.00 | 3015.74 |
| | Cultivated land | 31.09 | 284.17 | 60,336.69 | 195.52 | 542.35 | 14.47 | 61,404.30 |
| 2005–2010 | Forestland | 0.03 | 1.05 | 15.18 | 37,424.47 | 7.10 | 0.58 | 37,448.40 |
| | Grassland | 80.09 | 19.26 | 511.56 | 218.02 | 30,951.17 | 1.03 | 31,781.14 |
| | Water body | 0.24 | 0.05 | 4.49 | 0.19 | 0.50 | 108.99 | 114.46 |
| | Total | 831.80 | 3323.76 | 60,924.19 | 37,839.24 | 31,561.02 | 125.14 | 134,605.14 |

To be continued

Continued

| Period | | Bare land | Built-up land | Cultivated land | Forestland | Grassland | Water body | Total |
|---|---|---|---|---|---|---|---|---|
| | Bare land | 546.55 | 3.90 | 116.26 | 0.54 | 164.41 | 0.13 | 831.80 |
| | Built-up land | 0.00 | 3323.76 | 0.00 | 0.00 | 0.00 | 0.00 | 3323.76 |
| | Cultivated land | 20.10 | 353.17 | 59,947.23 | 119.64 | 466.57 | 17.47 | 60,924.19 |
| 2010–2015 | Forestland | 0.13 | 1.32 | 23.55 | 37,802.43 | 11.45 | 0.37 | 37,839.24 |
| | Grassland | 21.10 | 19.96 | 473.44 | 146.40 | 30,898.60 | 1.52 | 31,561.02 |
| | Water body | 0.28 | 0.02 | 3.28 | 0.21 | 0.35 | 120.99 | 125.14 |
| | Total | 588.16 | 3702.14 | 60,563.76 | 38,069.22 | 31,541.38 | 140.48 | 134,605.14 |
| Period | | Bare land | Built-up land | Cultivated land | Forestland | Grassland | Water body | Total |
| | Bare land | 503.83 | 7.02 | 45.48 | 0.26 | 31.46 | 0.10 | 588.16 |
| | Built-up land | 0.00 | 3702.14 | 0.00 | 0.00 | 0.00 | 0.00 | 3702.14 |
| | Cultivated land | 26.07 | 1025.93 | 58,830.17 | 177.73 | 487.87 | 15.99 | 60,563.76 |
| 2015–2020 | Forestland | 0.26 | 8.12 | 58.83 | 37,973.94 | 26.73 | 1.35 | 38,069.22 |
| | Grassland | 42.12 | 51.44 | 735.70 | 151.70 | 30,557.59 | 2.84 | 31,541.38 |
| | Water body | 1.69 | 1.59 | 3.34 | 0.17 | 0.37 | 133.32 | 140.48 |
| | Total | 573.97 | 4796.25 | 59,673.51 | 38,303.79 | 31,104.03 | 153.60 | 134,605.14 |
| Period | | Bare land | Built-up land | Cultivated land | Forestland | Grassland | Water body | Total |
| | Bare land | 141.64 | 2.45 | 477.52 | 9.95 | 467.65 | 11.63 | 1110.85 |
| | Built-up land | 0.00 | 1662.52 | 0.00 | 0.00 | 0.00 | 0.00 | 1662.52 |
| | Cultivated land | 177.51 | 3014.65 | 45,972.82 | 4013.84 | 9212.04 | 85.70 | 62,476.57 |
| 1985–2020 | Forestland | 2.09 | 21.35 | 1546.09 | 31,390.12 | 2739.03 | 11.19 | 35,709.87 |
| | Grassland | 249.99 | 89.12 | 11,650.04 | 2889.12 | 18,684.02 | 9.54 | 33,571.82 |
| | Water body | 2.73 | 6.16 | 27.04 | 0.75 | 1.28 | 35.55 | 73.52 |
| | Total | 573.97 | 4796.25 | 59,673.51 | 38,303.79 | 31,104.03 | 153.60 | 134,605.14 |